JOURNAL OF GEOPHYSICAL RESEARCH VOL. 68, NO. 13 JULY 1, 1963

Variations of the Proton Energy Spectrum with Position in the Inner Van Allen Belt

J. E. NAUGLE AND D. A. KNIFFEN

NASA Goddard Space Flight Center, NASA Greenbelt, Maryland

Abstract. A cylindrical stack of nuclear emulsions was flown in the payload section of a research rocket into the northern edge of the inner part of the Van Allen radiation region on September 19, 1960. The emulsion stack was shielded inside a tungsten cassette and was then exposed to the ambient radiation by rotation behind a window in the wall of the cassette covered with a 0.04-g/cm² aluminum shield. In this way it was possible to make a detailed study of the energy spectrum of the trapped particles at various positions in space. The rocket trajectory covered L values ranging from about 1.45 to $1.85R_E$. Five points along the trajectory were chosen for analysis, and the differential and integral proton energy spectrums were obtained for each point. Above 30 Mev in all cases, and below 30 Mev at the lower L values, the proton energy spectrums were in agreement with previous experiments; however, there was a sharp change in the slope of the spectrums with a steeper slope ($j(E) = KE^{-4.5}$) at the higher L ($L > 1.6R_E$) values than had been expected on the basis of previous experiments and the galactic cosmic ray neutron albedo theory. The data for each of the points are presented, and the results are discussed. No particles of mass greater than the proton were observed in a particle composition study averaged over the trajectory. An upper limit is presented for heavier particles in the trapped radiation.

Introduction. The work of *Van Allen et al.* [1958] and others demonstrated the existence of the trapped radiation region in the vicinity of the earth and showed that there are large variations in intensity with position. *Freden and White* [1960, 1962] and *Armstrong et al.* [1961] have shown the presence of penetrating protons in the inner zone and have measured their energy spectrum averaged over an ICBM trajectory from Cape Canaveral.

The emulsion experiments by Freden and White and by Armstrong et al. were limited in the amount of information that could be obtained, because they were hitchhikes on military vehicles. The lowest energy that could be detected was determined by the thickness of the nose cone. There was no mechanism to determine the flux as a function of position in the belt. The early satellite experiments could accurately measure the flux as a function of position but could not differentiate between electrons and protons or measure their energy. The present experiment was conceived to make use of the nuclear emulsion properties to determine accurately not only the number of particles but also their velocity, mass, and charge as a function of position. For this purpose a special nose cone, the NERV (nuclear emulsion recovery vehicle), was developed, flown, and recovered successfully on the first attempt, September 19, 1960. To measure the variation of the flux over the greatest possible region of the belt, the rocket was flown on a special trajectory from the Pacific Missile Range which carried it along a magnetic meridian into the inner belt. Preliminary results of the experiment have already been published [*Naugle and Kniffen*, 1961].

The spatial and temporal variations of j are required to map out the radiation levels in the belts adequately as well as to determine the source or sources of the particles, their lifetimes in the trapped region, the mechanism limiting the intensities of the belts at higher altitudes, and various other features of the belts.

Several authors [*Singer*, 1958; *Vernov et al.*, 1959; *Hess*, 1959] have suggested the decay protons of cosmic ray neutron albedo as at least a partial source of the protons in the inner belt. *Lenchek and Singer* [1962] and *Lenchek* [1962] have also calculated the effect of a solar cosmic ray neutron albedo source. An abundance of more recent data [*Freeman*, 1962; *Bame et al.*, 1961; *Davis*, 1962; *Pizella et al.*, 1962; *Imhof et al.*, 1962] indicates that there must be addi-

tional sources of intense numbers of protons down to energies of a few kilo electron volts in both the inner and the outer belts. Both direct injection and local acceleration have been suggested as possible sources, but as yet there is no quantitative explanation of the observed spectrums in this energy region.

Several loss mechanisms have been presented to explain the absence of trapped particles at higher energies at greater distances from the earth. *Singer* [1959] and *Lenchek and Singer* [1962] have suggested that the adiabatic invariance of the magnetic moment will break down at a momentum such that the radius of gyration of the proton is comparable to the dimensions of the inhomogeneities in the magnetic field. *Welch and Whitaker* [1959], *Dragt* [1961], and *Wentzel* [1961] have suggested that hydromagnetic waves scatter the more energetic particles magnetically, causing them to mirror lower in a more dense atmosphere and be removed. Other mechanisms, such as an instability of the earth's magnetic field [*Gold*, 1959], the effect of the large magnetic anomaly at Capetown [*Dessler*, 1959], and absorption by interstellar dust [*Lenchek and Singer*, 1962], have also been suggested.

The purpose of this paper is to discuss the results of the NERV experiment more completely and to compare the predictions of the various theories of the origin, acceleration, and loss mechanisms of the trapped protons with these results.

Description of the experiment. The experiment consisted of a cylindrical stack of 20-Ilford G-5 and G-2 nuclear emulsions. The stack was encased in a tungsten emulsion container with a wall at least 30.6 g/cm² thick everywhere except for a port, 1 cm² in area, on the side of the container. The port was covered by aluminum foil 0.04 g/cm² thick.

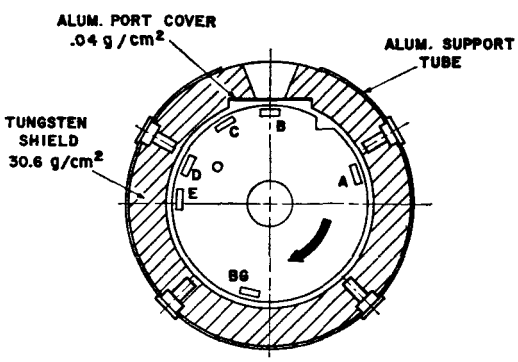

Fig. 1. Cutaway top view of the nuclear emulsion container. Film position at apogee.

Figure 1 shows the arrangement. The emulsion stack began rotating at liftoff of the rocket at a constant rate of 0.221° ± 0.001°/sec. It rotated for 1440 seconds, turning through 318°. Each exposed point on the periphery of the stack was behind the port for 79 seconds, and behind 30.6 g/cm² of tungsten for the remainder of the flight. The regions labeled *A*, *B*, *C*, *D*, and *E* in Figure 1 represent areas that were scanned to measure the spectral intensity at a given time during the flight. The track population in these regions is made up of tracks of particles that came through the port during the 79-second exposure and a background of particles that passed through the tungsten during the remaining time the payload was in the radiation belt. The region of the stack labeled *BG*, which did not pass behind the port, has been used to measure this background.

This arrangement improved upon previous emulsion experiments in two respects. The rotating emulsion made it possible to determine the time, and hence the position, at which a given particle had entered the emulsion. The very thin window over the port, together with the arrangement for extending the emulsion container outside the nose cone, lowered the detection threshold from the 70 Mev in previous experiments down to about 8 Mev in this experiment. Protons of energy $\geq$8 Mev could penetrate the port and be detected in the emulsions, whereas only protons with energy $\geq$145 Mev could penetrate the tungsten and be detected.

The emulsion container was an integral part of the special nuclear emulsion recovery vehicle (NERV). It was designed to permit the 4-inch cylindrical container to be extended through the front of the vehicle so that the emulsion container and its port could be exposed directly to the ambient radiation. Figure 2 is a side view of experimental arrangement showing the emulsion container in its extended position. Figure 3 is a cutaway view showing the extended emulsion container and the remainder of the nose cone. The nose cone was covered with an ablation material which, together with the mass of the tungsten, kept the emulsions at 70 ± 10°F throughout the flight, including re-entry.

Figure 4 is a plot of the energy a radial proton

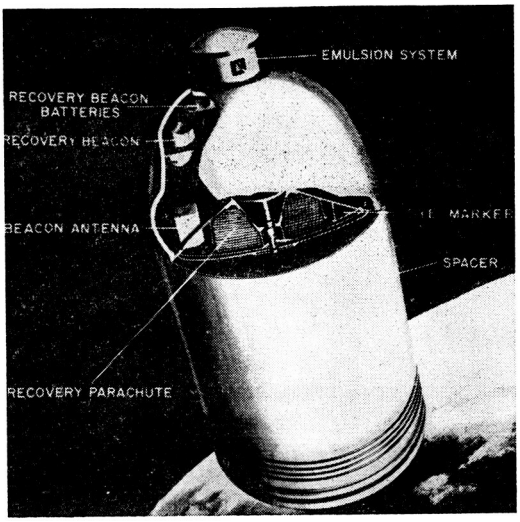

Fig. 3. Cutaway view of the nuclear emulsion recovery vehicle with the remainder of the nose cone (emulsion container extended).

radar data it was also possible to determine the direction of the spin axis during burning of the fourth stage. With this orientation of the spin axis and the assumption that the spin axis remained fixed in inertial space it was possible to reconstruct the angle γ between the spin axis of the rocket and the local magnetic field vector. The value of γ at each location is given in Table 1. In general, the spin axis was initially nearly parallel to the local magnetic field vector, but as the payload traveled along its trajectory this angle steadily increased to 40° at point E as shown in Figure 6.

Figure 7 shows the relations between the spin axis of the rocket, the plane of the emulsions, the dip angle of the track relative to the emulsion, and the pitch angle α' of the particles with respect to the local magnetic field vector **B** at the location of the measurement. Viewed in a coordinate system fixed in the spacecraft the magnetic field **B** will appear to rotate about the axis of the rocket. A particle with a given dip angle β in the emulsion will have had a pitch angle α' between $(90° - \beta) \pm \gamma$, depending on the time during a roll period that it entered the emulsion.

At a particular geomagnetic latitude, only a limited range of pitch angles is available, $\alpha_C' \leq \alpha' \leq 90°$, where α_C' is the pitch angle of a particle at the location of the measurement which mirrors at the lower edge of the belt on the particular shell on which the measurement was made. Because the measurements were made at geomagnetic latitudes $\geq 25°$, only a limited range of equatorial pitch angle distribution could be studied in this experiment. The pitch angle at the equator α is related to the pitch angle α' measured at the geomagnetic latitude λ by the relation

$$\alpha = \cos^{-1} \cdot \left[1 - (1 - \cos^2 \alpha') \frac{\cos^6 \lambda}{(4 - 3 \cos^2 \lambda)^{1/2}} \right]^{1/2} \quad (1)$$

α_C and α_{90}, the pitch angles at the equator corresponding to $\alpha' = \alpha_C'$ and to $\alpha' = 90°$, respectively, are given in Table 1.

Figure 8 shows how a particular pitch angle distribution at the equator will appear at various geomagnetic latitudes. The exact variation of j with pitch angle and L for these energy ranges has not yet been measured directly. *Davis* [1962] has found that j is of the form $j = k \sin^3 \alpha$ for protons between 1 and 4 Mev. Using the relation derived by *Ray* [1960], it is found that $j = k \sin^{2.5} \alpha$ by analysis of the omnidirectional intensity J_0. Therefore, Figure 8 is a reasonable approximation to the expected pitch angles studied in this experiment.

Figure 8 and Table 1 show that it is possible to explore only a very limited part of the pitch angle distribution at the equator on a flight like this at a high geomagnetic latitude. As Table 1 shows, all the particles observed on this flight have their pitch angles, at the equator, contained

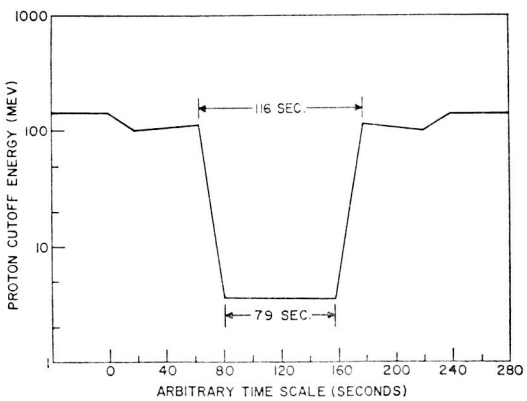

Fig. 4. The energy a radial proton must have to penetrate the shield and be detected in the emulsion as a function of time as the emulsion rotates behind the port.

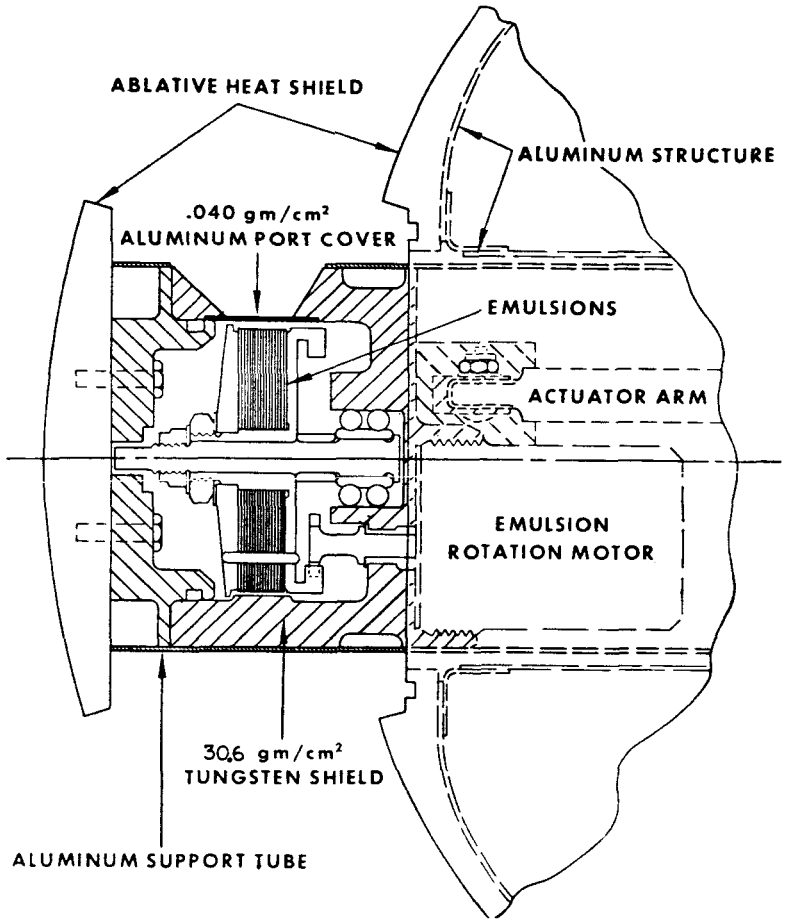

Fig. 2. Cutaway side view of the experimental arrangement with emulsion container in extended position.

must have to penetrate the tungsten shield and be detected in the emulsion as a function of time during the passage of a point on the periphery of the emulsion behind the port.

Flight details. The rocket was launched at 1635 UT, September 19, 1960, from Point Arguello, California. The launch azimuth of 193° was chosen so that the flight path would parallel a magnetic meridian. The nose cone was recovered at 1923 UT at 15°N latitude and 126°12′W longitude.

Figure 5 is a meridian section containing the rocket trajectory. The dashed lines are the magnetic lines of force based on the *Finch and Leaton* [1957] coefficients. The solid lines are the contours of constant integral omnidirectional intensity for protons of energy >30 Mev based on data furnished by the Iowa Group (C. E. McIlwain, private communication). The lettered points are the locations along the trajectory at which the correspondingly lettered regions of the emulsion in Figure 1 were behind the port.

Each of the lettered points has been analyzed. Table 1 gives the altitude H, the geomagnetic latitude λ, the value of the scalar magnetic field B, and L (the parameter used by *McIlwain* [1961] to specify a magnetic shell) at each of these locations along the trajectory.

The payload was spin-stabilized after leaving the atmosphere, the spin axis of the rocket remaining fixed in inertial space. NERV did not contain sensors for the determination of the position or orientation of the rocket, but the payload was tracked by FPS-16 radar to determine the rocket's trajectory. From the analysis of the

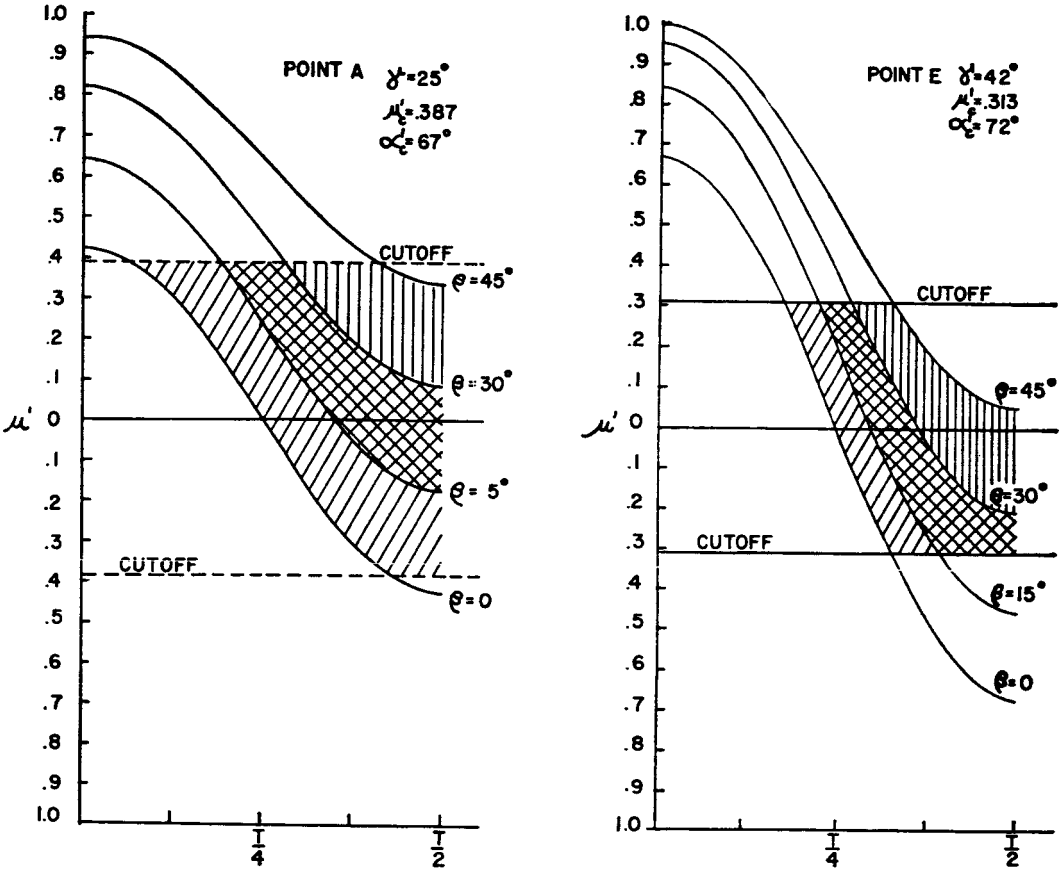

Fig. 9. Variation of the pitch angle $\mu' = \cos \alpha'$ for a given value of dip angle β with time during a roll period. The variation is plotted for $\gamma = 25°$ and $\gamma = 42°$, corresponding to locations A and E, respectively. The cutoff $\mu_c' = \cos \alpha_c'$ corresponds to an altitude (or B value) on a particular L shell below which satellite data show no particles mirroring.

Because of the high background and the low minimum blob density, we could not reliably detect particles at minimum ionization. Therefore, in all the results reported in this analysis, we have used only tracks with blob densities ≥ 20.

All tracks that at the scan line were within $\pm 45°$ of the plane of the emulsion and within $\pm 25°$ of a radius vector in the plane of the emulsion were recorded and were used to evaluate the integral fluxes. Then tracks that, on the basis of dip measurement at the scan line alone, would have traversed a track length of at least 2.5 mm before leaving the emulsion, independent of energy considerations, were chosen to obtain the energy measurements as described below.

The part of the emulsion labeled *BG*, which was not exposed behind the port, was also scanned with the same criteria to obtain a background correction for the exposed regions of the emulsions.

The scanning to study composition was made in the G-2 emulsion. This allowed tracks to be grain-counted within 200 microns of the end with good resolution between protons, deuterons, tritons, and α particles down to energies of 14 Mev for deuterons, 16 Mev for tritons, and 40 Mev for α particles.

More than 500 protons were used to establish the grain-density ionization curves for the G-2 emulsions. The grain-density curve for protons was established, and by means of this curve theoretical grain-density versus range curves were constructed for heavier particles by using

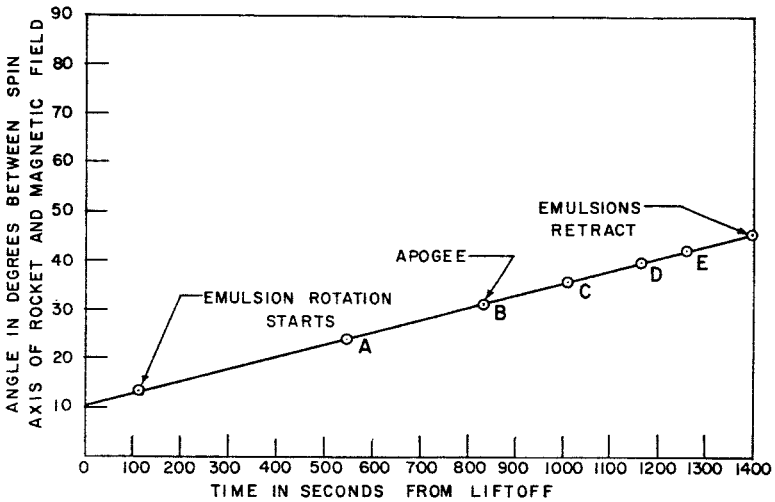

Fig. 6. Variation of the angle between the spin axis of the rocket and the local magnetic field vector as a function of time after rocket liftoff.

using an exposure time $t = f\,\Delta t_k$, where Δt_k is the effective time the emulsion was behind the port.

Scanning criteria. Line scans were made at points A, B, C, D, and E. They were made at 600, 1200, and 2400 microns from the edge of the emulsions; because of blackening it was not possible to scan closer than 600 microns to the edge, but they were made as close to the edge as possible in order to extend the spectrum to the lowest possible energy. However, owing to excess background grains from low-energy electrons, tracks of blob density $b \leq 30$ blobs/100 microns ($\geq$175-Mev protons) could not be detected at 600 microns from the edge. The scanning efficiency for tracks with $b \geq 20$ ($\leq$360-Mev protons) at 1200 microns from the edge as checked by rescans was 100 per cent. For a particle at minimum ionization b was about 14.

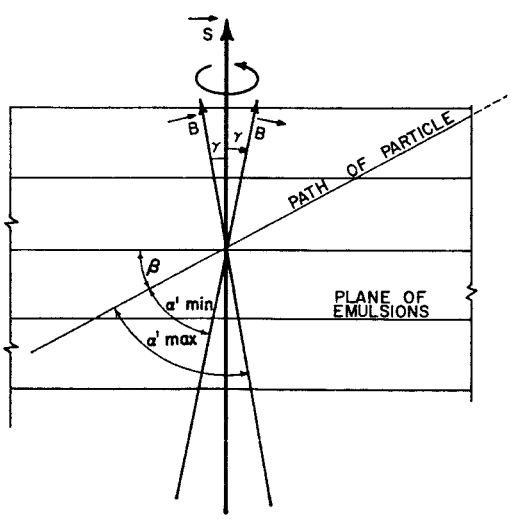

Fig. 7. Schematic diagram showing the relation between the dip angle of the track, β; γ, the angle between the spin axis of the rocket **S** and the magnetic field **B**; and α', the pitch angle of the particle.

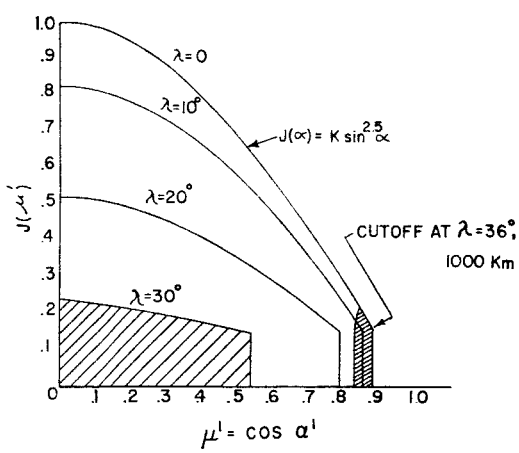

Fig. 8. Plot showing how a particular pitch angle distribution changes with geomagnetic latitude. The shaded area under $\lambda = 30°$ corresponds to the range of pitch angles accessible in this experiment, and transforms at the equator into the smaller shaded area at $\mu = 0.85$.

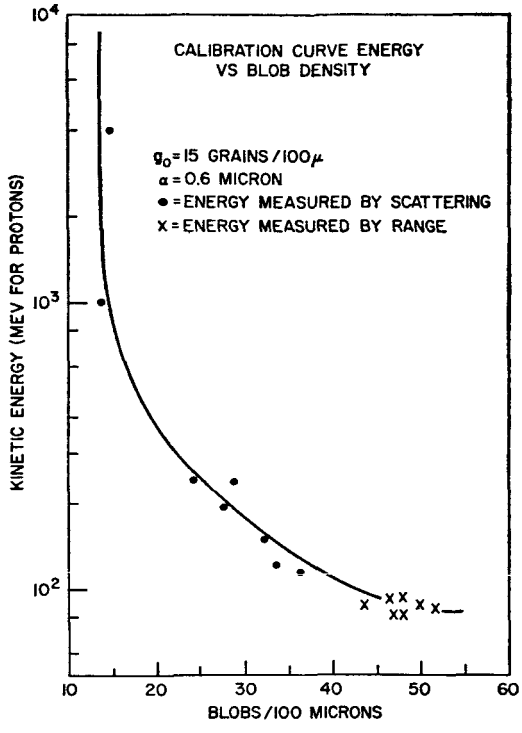

Fig. 10. Energy versus normalized blob density.

the value of the grain density of a proton of the same ionization. The theoretical curves were then checked by grain counts on heavy particles from interaction stars. The measured grain densities agreed with the theoretical curve well within the statistical error.

The mass distribution was next determined by selecting, on the basis of dip angle alone, 500 tracks having a possible track length of at least 1 mm. Each track was grain-counted at the scan line and at a fixed distance from the end of the track. Tracks that did not end were discarded, so that a small bias was introduced in favor of heavier particles, owing to the loss of lighter particles by scattering. However, very few particles were eliminated by this criterion, since most of the particles were of low energy and had short residual ranges. In addition, an upper energy cutoff was introduced in the form of a 4-mm residual range cutoff. Therefore, the mass distribution covers protons in the 12- to 31-Mev range, deuterons in the 14- to 42-Mev range, and α particles in the 40- to 125-Mev range.

Determination of the energy. The variation of blob density with energy was determined primarily from scattering measurements and blob counts on ending protons. The assumption was made that the grain density varied with energy according to the Fowler-Perkins law [*Fowler and Perkins*, 1955]. The blob counts and scattering measurements were made on long, flat tracks. Applying the relation between grain density and blob density $b = ge^{-\delta g}$, where δ is an approximation to the grain size and g is the grain density, a best fit was made to the experimental points taking the minimum blob density as a parameter. A value of $b_0 = 14$ was obtained.

Figure 10 is a plot of energy versus blob density. The crosses are experimental points based on protons that ended in the emulsion; the dots are based on scattering data.

All particles in the scans that had a $b \geq 20/100$ microns and a possible path length in the emulsion at the scan line of at least 2.5 mm, on the basis of dip angle alone, were followed at least 2.5 mm, and a preliminary blob count was made.

Black tracks and gray tracks with $b \geq 40$ were followed until they either ended or interacted with the emulsion. Their energy was determined from their range in emulsion [*Atkinson and Willis*, 1957]. Approximately 70 per cent of the tracks ended in the emulsion at points A, B, and C, and essentially all tracks with energies less than about 70 Mev ended. In contrast, only about 30 per cent of the tracks ended at points D and E, emphasizing the relative dirth, at these points, of particles with lower energies.

The energy of particles with $20 \leq b \leq 30$ was determined by scattering, and the energy of those with $30 \leq b \leq 40$ by blob density.

It was not possible to obtain a direct cross calibration of all three techniques for energy determination by simultaneously measuring the scattering and blob density as a function of range, since protons with kinetic energies greater than 170 Mev could not be stopped in the emulsion. However, Figure 10 shows that the three techniques are self-consistent. If they were not, the experimental points would not lie along the theoretical curve. In the overlapping areas of the three techniques cross checks were made, and the energies measured by different techniques were all well within the experimental errors.

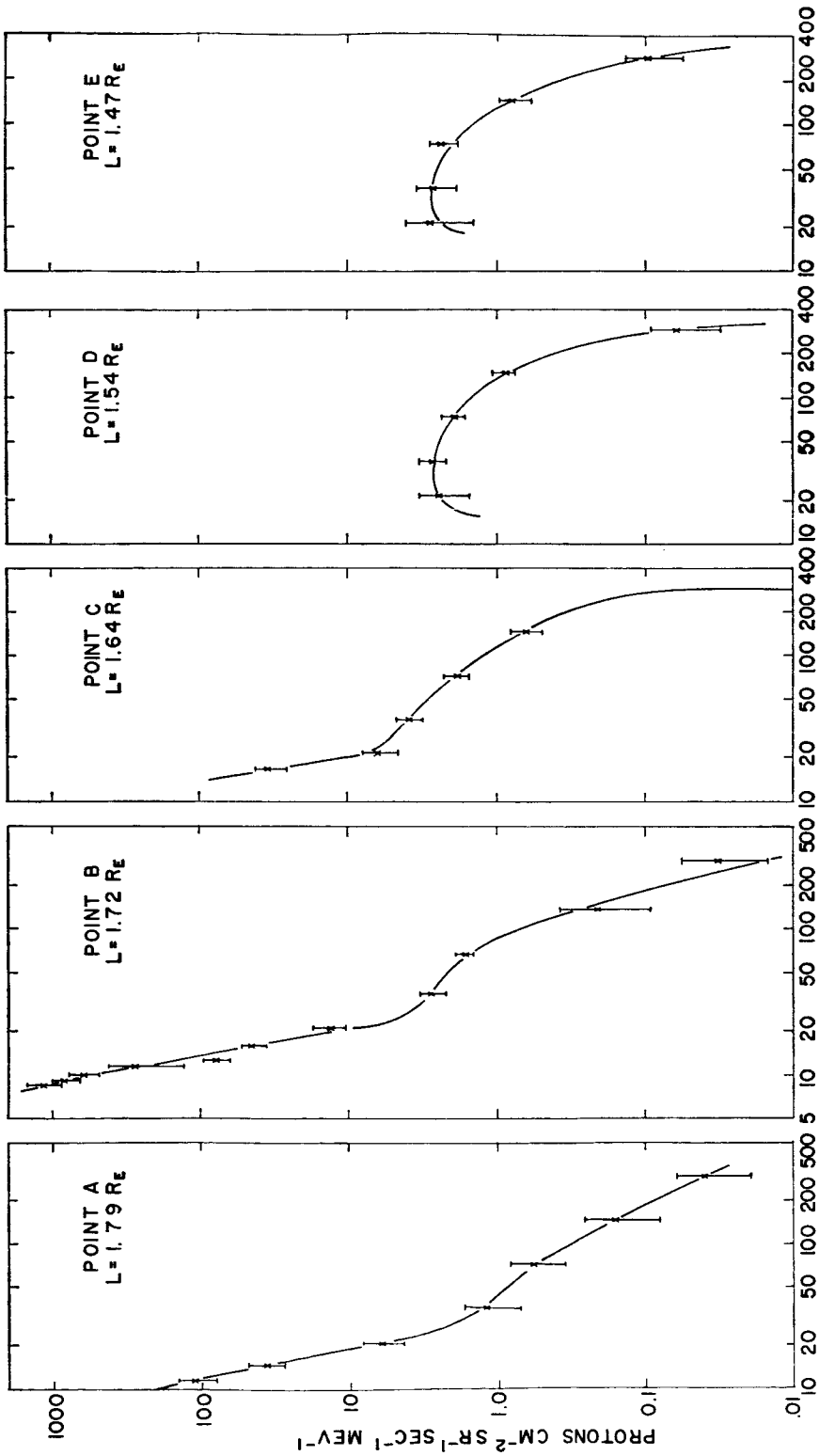

Fig. 11. Differential energy spectrums obtained at the five locations.

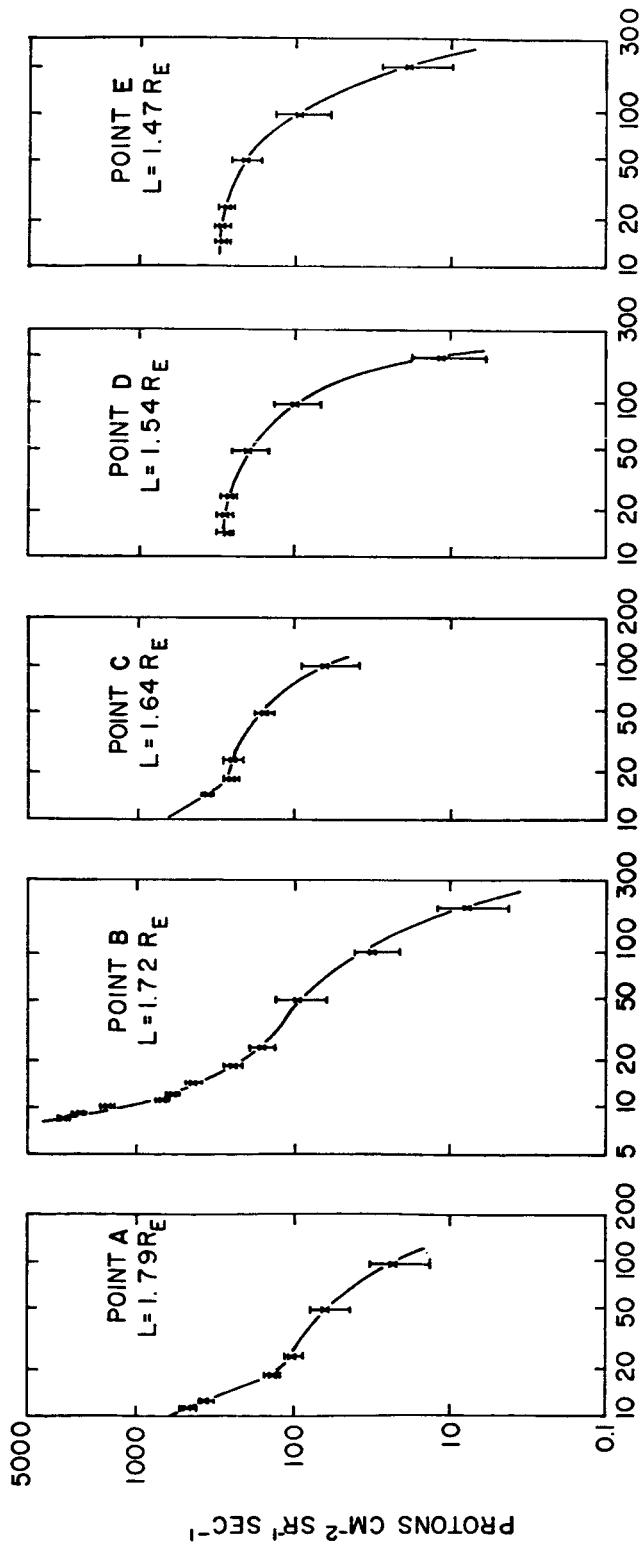

Fig. 12. Integral energy spectrums obtained at the five points.

30 Mev), the integral unidirectional flux of protons of energy $\geq$30 Mev, is obtained and can be compared directly with that observed by Van Allen et al. [*McIlwain*, 1961] at the same point as shown in Table 2. The agreement between the two is quite good at points *B*, *C*, and *D* and not quite so good at points *A* and *E*, although slight errors in the location of the measurement and the rapid variation of the flux with altitude could account for the differences at *A* and *E*. For instance, if *B* at point *E* were in error by 0.01 gauss, there would be a factor-of-3 variation in the expected integral flux.

The lack of particles below 24 Mev at points *D* and *E* is real, since energies down to 12 Mev were detectable within the scan criteria. However, the numbers of particles found were so few that the intensity fell below the scale of the graphs.

Discussion of the results. The most pronounced feature of the various spectrums is the systematic variation in the shape of the spectrum with position. This unexpected result indicates that, in the energy region below 30 Mev, the galactic neutron albedo theory cannot account for the shape of the spectrum or its behavior with position. This theory [*Freden and White*, 1962] would predict a dip in the energy spectrum below 30 Mev due to an increased neutron absorption at these energies by the nitrogen and oxygen in the upper atmosphere. This absorption mechanism would account for the maximum in the energy spectrum at 30 Mev at points *D* and *E* and the plateau in the spectrum at the same energy that is observed at point *B*. However, although this theory can explain the paucity of protons below 30 Mev at the low *L* values (points *D* and *E*), it cannot explain the copious numbers of protons below 30 Mev observed at the higher *L* values (points *A*, *B*, *C*) in this and other experiments [*Bame et al.*, 1961; *Davis*, 1962].

There are several mechanisms by which such a steep spectrum can be obtained at these energies; however, the high intensities of particles require a stronger source of protons than could be provided by the galactic cosmic ray neutron albedo spectrum measured by *Hess et al.* [1959]. There might be a serious dilemma in deciding among the various possible explanations of the combined steep spectrum and high intensities in the 8- to 30-Mev region were it not for the fortunate circumstance that the trajectory of the rocket passed through the quasi-boundary between points *C* and *D* where this component of the spectrum disappeared.

This feature gives an additional criterion with which to seek the source of protons giving rise to this form of spectrum. From Figure 12 it can be seen that the slope of the proton spectrum between 16 and 48 Mev changes rapidly beginning at an *L* value of about 1.55 with relatively few of the low-energy protons present below this value of *L* and a great abundance of them above it. Thus we must look for an intense source of low-energy protons that has access only to higher magnetic shells. This type of spectrum could reasonably be expected from a source of protons that come from the decay of neutrons arising from the interaction of low-energy solar protons with the earth's atmosphere over the polar regions. A sufficiently intense source of such particles is known to arrive at the earth after certain types of solar flares [*McDonald*, 1962].

Such an explanation of the spectral variations at low energies was suggested in the preliminary results of this experiment [*Naugle and Kniffen*, 1961; *Lenchek and Singer*, 1962].

Subsequently, quantitative calculations to determine the feasibility of such an explanation were made by *Lenchek* [1962]. He calculates from a time-averaged solar cosmic ray spectrum the neutron spectrum to be expected as the solar corpuscular particles collide with the earth's upper atmosphere. Assuming adiabatic trapping, he calculates the injection coefficients for the various locations, the pitch angles, and the lifetimes, and he shows that this spectrum could be an essentially time-invariant feature of the

TABLE 2. Comparison of Counter and Emulsion Fluxes

Location	J ($\geq$31 Mev), cm^2 sr sec	J_0 (31 Mev), cm^2 sec	J_0* (31 Mev), cm^2 sec
A	90	440	220
B	180	1160	1000
C	220	1360	1600
D	230	1230	1290
E	250	1000	390

* Satellite data from C. E. McIlwain, private communication.

trapped proton spectrum in the allowed regions. His calculated spectrum and its variation with position are in fair agreement with the spectrum observed at points *A*, *B*, and *C* in this experiment, providing good evidence in support of this type of source for the steep low-energy component since it is the only apparent explanation of the absence of low-energy protons at the lower *L* values. Conclusive evidence for this source, however, cannot be obtained until there is a complete study of the variation of the trapped proton energy spectrum as a function of the pitch angle at the equator, or any of the alternative measurements that can provide these data.

Bame et al. [1961] and *Davis* [1962] have shown that, at high *L* values, the proton energy spectrum continues to rise steeply down to about 0.1 Mev. *Freeman* [1962] has observed an extremely high flux of very-low-energy protons in regions of *L* value from which solar protons are excluded. The intensity of this low-energy component is so high that it appears impossible, with reasonable lifetimes, to account for it from either the galactic or solar cosmic ray source. Thus, it appears that there may be at least three sources for trapped protons: galactic cosmic rays for the high-energy protons at all *L* values; solar cosmic rays for the low-energy (1- to 30-Mev) protons at high *L* values; and some as yet unknown accelerating mechanism for the very-low-energy (0.1- to 1-Mev) protons.

Because there is such a large background correction to the data above about 100 Mev the errors on the data points are quite large. This is due to the collection over the entire periphery of the emulsions of particles that penetrate the tungsten shielding during the entire time of flight. Thus it is only possible to say that at higher energies the gross shape of the spectrum remains essentially the same and there is evidence for a decrease of intensity at the higher *L* value. However, there are not sufficient data to give new information about the loss mechanism for trapped particles.

At comparable positions the data at the high energies are in agreement within a factor of 2 with previous results [*Freden and White,* 1962; *Armstrong and Heckman,* 1962], which is as good as should be expected in view of the differences in trajectory and exposure technique.

In a study of 500 tracks to investigate particle composition in the proton range interval corresponding to 12 to 31 Mev, no particles of mass greater than the proton were found. For a sample of this size there is only a 5 per cent probability that the observer would expect three heavier particles and obtain none. Thus the heavier particles due both to primaries and to secondaries from interaction in the tungsten make up less than 0.6 per cent of the entire population of observed tracks, and so this can safely be taken as an upper limit to the number expected from primaries alone.

Summary

1. At *L* values above about $1.6R_E$ the slope of the proton energy spectrum below about 30 Mev is very steep compared with predictions of the galactic cosmic ray neutron albedo theory and is most probably due to solar cosmic ray neutron albedo; however, the flux of trapped protons with energies greater than about 30 Mev is in agreement with the predictions of this theory.

2. The shape and flux of the spectrum vary with latitude, points *A* and *D* being at the same altitude.

3. At comparable positions in the radiation region the results are in reasonable agreement with previous measurements.

4. On the basis of these and subsequent data, it appears that there must be at least three sources of trapped protons.

5. The flux of geomagnetically trapped particles heavier than protons in the proton energy range of 12 to 30 Mev is less than 0.6 per cent of the total flux, on the date and at the locations studied in this experiment.

Acknowledgments. An experiment like this, which required recovery at sea, would not have been successful without the superior performance and cooperation of so many people that, because of the limitations of space, we cannot acknowledge them individually. Charles Campbell, project engineer, and Gerald Longanecker, assistant project engineer, each made major contributions which ensured the success of the project.

References

Armstrong, A. H., F. B. Harrison, H. H. Heckman, and L. Rosen, Charged particles in the inner Van Allen radiation belt, *J. Geophys. Res., 66,* 351–357, 1961.

Armstrong, A. H., and H. H. Heckman, Energy